The FEBS Journal

FEBS PRESS science publishing by scientists

Invisible detergents for structure determination of membrane proteins by small-angle neutron scattering

Søren Roi Midtgaard[1], Tamim A. Darwish[2], Martin Cramer Pedersen[1,3], Pie Huda[1], Andreas Haahr Larsen[1], Grethe Vestergaard Jensen[1], Søren Andreas Røssell Kynde[1], Nicholas Skar-Gislinge[1], Agnieszka Janina Zygadlo Nielsen[4], Claus Olesen[5], Mickael Blaise[6,7], Jerzy Józef Dorosz[8], Thor Seneca Thorsen[8], Raminta Venskutonytė[8], Christian Krintel[8], Jesper V. Møller[9,10], Henrich Frielinghaus[11], Elliot Paul Gilbert[12], Anne Martel[13], Jette Sandholm Kastrup[8], Poul Erik Jensen[4], Poul Nissen[10,14] and Lise Arleth[1]

1 Structural Biophysics, X-ray and Neutron Science, The Niels Bohr Institute, University of Copenhagen, Denmark
2 National Deuteration Facility, Australian Nuclear Science and Technology Organization, Lucas Heights, Australia
3 Department of Applied Mathematics, Research School of Physics and Engineering, Australian National University, Canberra, Australia
4 Copenhagen Plant Science Center, University of Copenhagen, Denmark
5 Department of Biomedicine, Aarhus University, Denmark
6 Institut de Recherche en Infectiologie de Montpellier, CNRS, Université de Montpellier, France
7 Centre for Carbohydrate Recognition and Signaling, Department of Molecular Biology, Aarhus University, Denmark
8 Department of Drug Design and Pharmacology, Faculty of Health and Medical Sciences, University of Copenhagen, Denmark
9 Department of Biomedicine, Aarhus University, Denmark
10 Department of Molecular Biology and Genetics, Centre for Membrane Pumps in Cells and Disease – PUMPkin, Danish National Research Foundation, Aarhus University, Denmark
11 Forschungszentrum Jülich GmbH, TUM FRM-2, Garching, Germany
12 Australian Centre for Neutron Scattering, Australian Nuclear Science and Technology Organization, Lucas Heights, Australia
13 Institut Laue-Langevin, Grenoble, France
14 DANDRITE, Nordic-EMBL Partnership for Molecular Medicine, Aarhus University, Denmark

Keywords
contrast matching; deuteration; membrane proteins; SANS; Small-angle neutron scattering

Correspondence
S. R. Midtgaard and L. Arleth, Structural Biophysics, X-Ray and Neutron Science, Niels Bohr Institute, University of Copenhagen, Universitetsparken 5, DK-2100 Copenhagen, Denmark
Emails: soromi@nbi.ku.dk (S.R.M.); arleth@nbi.ku.dk (L.A.)
and
T. Darwish, Australian Nuclear Science and Technology Organisation, Locked Bag 2001, Kirrawee DC, NSW 2232, Australia
Email: tde@ansto.gov.au
and
P. Nissen, Aarhus University, Gustav Wieds Vej 10, 8000, Aarhus C, Denmark
Email: pn@mbg.au.dk

(Received 10 July 2017, revised 20 October 2017, accepted 21 November 2017)

doi:10.1111/febs.14345

A novel and generally applicable method for determining structures of membrane proteins in solution via small-angle neutron scattering (SANS) is presented. Common detergents for solubilizing membrane proteins were synthesized in isotope-substituted versions for utilizing the intrinsic neutron scattering length difference between hydrogen and deuterium. Individual hydrogen/deuterium levels of the detergent head and tail groups were achieved such that the formed micelles became effectively invisible in heavy water (D_2O) when investigated by neutrons. This way, only the signal from the membrane protein remained in the SANS data. We demonstrate that the method is not only generally applicable on five very different membrane proteins but also reveals subtle structural details about the sarco/endoplasmatic reticulum Ca^{2+} ATPase (SERCA). In all, the synthesis of isotope-substituted detergents makes solution structure determination of membrane proteins by SANS and subsequent data analysis available to nonspecialists.

Introduction

Biological membranes form the barrier between internal and external environments of cells and create the separation of compartments and organelles within the cell. They are functionalized by a plethora of membrane proteins that include structural proteins, receptors, channels, active transporters and proteolytic enzymes. Studies of the structure and conformational changes related to the function of membrane proteins therefore represent very important problems in molecular cell biology. Structural studies usually require that the membrane protein of interest is removed from the native membrane, isolated and purified to homogeneity. This requires that the amphipathic membrane protein is stabilized in solution. Multiple systems, including traditional detergents [1], bicelles [2,3], peptide discs [4], amphiphilic polymers [5,6] and nanodiscs [7] are available for this purpose. While detergents and bicelles have been useful for Cryo-EM [8], NMR [9] and crystallization experiments [1], the comparatively monodisperse nanodisc particles are promising in combination with small-angle scattering and allows low-resolution structural information of the membrane protein to be obtained under solution conditions [10–12]. However, reconstitution of membrane proteins in nanodiscs remains a challenge with respect to obtaining sufficiently homogeneous samples for scattering experiments. In our attempt to find a more general and easily applicable solution to these problems, the use of detergents was re-examined and combined with our previously developed idea of a "stealth"-carrier for SANS studies of membrane proteins [10]. The detergents, octyl β-D-glucopyranoside (OG) and n-dodecyl-β-D-maltopyranoside (DDM) that are both compatible with membrane protein reconstitution were deuterated through a new synthesis method that allowed for selective deuteration of the two detergents to different predetermined levels at the hydrophilic head groups and hydrophobic tails. To obtain the best possible SANS signal-to-noise of the membrane protein structure, the different parts of the detergents were deuterated such that they had the same neutron scattering length density as 100% deuterium oxide (D_2O). This way, the obtained SANS data of membrane proteins stabilized in these detergents in D_2O only consists of the single contrast signal stemming from the purified membrane protein.

The general idea to use the contrast match point of a detergent or surfactant to study membrane protein structures has previously been investigated [13–29]. However, a common feature for all previous studies is that they rely on commercially available hydrogenated detergents or fully deuterated detergents developed for different purposes. This is reflected in the resulting neutron scattering data, which include scattering cross-terms from the entire detergent–membrane protein complex due to the differences in excess scattering length density of the hydrophobic and hydrophilic parts of the detergents present on length scales of 10–20 Å. This effect is difficult to disentangle from the signal from the membrane protein and significantly limits the resolution that can be obtained. In addition, the overall match point of the commercially available detergents is generally different from that of 100% D_2O, hence yielding additional incoherent scattering background from the hydrogen atoms in the buffer. While the studies have provided overall shape parameters of studied membrane proteins [14,20,21,24,27,28], their finer structure could not be extracted from the data due to these factors.

In this study, two commonly used detergents, OG and DDM, were synthesized with varying deuteration levels in head- and tail groups such that they were fully match-out in D_2O buffer when investigated by SANS. This yielded SANS data where only the membrane proteins were visible. The practical workflow is outlined in Fig. 1.

Initially, the membrane protein is purified in hydrogenated buffer and hydrogenated detergent. This step ensures that as many impurities as possible are removed before the more expensive deuterated buffers are introduced. Afterwards, a size exclusion purification in the equivalent deuterated buffer and match-out deuterated detergent is performed. This step ensures that the hydrogenated detergent and buffer are fully exchanged to the deuterated counterparts (see SI 3 for details). Furthermore, any aggregated protein that might be present in the sample arising from, for example, freezing and transport, is also removed to ensure optimal data quality. The peak fraction from the buffer and detergent exchange is collected and, without further manipulation, measured by SANS. Scattering data obtained this way can be reduced and

Abbreviations

bR, bacteriorhodopsin; Cryo-EM, Cryo Electron Microscopy; DDM, n-dodecyl-β-D-maltopyranoside; D_{max}, maximum distance; FWHM, full width half maximum; GluA2, ionotropic glutamate receptor A2; kDa, kilo dalton; LamB, maltoporin; MW, molecular weight; OG, octyl β-D-glucopyranoside; PSI, photosystem I; R_g, radius of gyration; SANS, small-angle neutron scattering; SAXS, small-angle X-ray scattering; SEC, size exclusion chromatography; SERCA, sarco/endoplasmatic reticulum Ca^{2+} ATPase; SI, supplemental information.

subsequently analysed by a number of available programs for small-angle scattering (such as ATSAS [30], WillItFit [31], SASSIE [32], IRENA [33], FoXS [34] etc.) due to the simplified contrast situation achieved through the use of *de facto* invisible detergents.

Results

Detergent deuteration

As described above, the chosen deuterated detergents were two commonly used sugar-based detergents, namely OG and DDM. The partial specific molecular volumes of the hydrophilic head and hydrophobic tail groups were determined by densitometry (see Supporting Information 1 for details) such that the deuteration level for complete match-out at 100% D_2O at 20 °C could be calculated (see Table 1). Custom syntheses were then developed to produce the desired partially deuterated versions of both detergents.

Synthesis of detergents with controlled deuteration levels in hydrophilic head groups and hydrophobic tails

Each of OG and DDM is made of two parts; the C8 or C12 alkyl chain tail and the corresponding sugar head of glucose or maltose respectively. In the case of OG, the required deuteration levels in the octyl chain and the glucose sugar head (seven nonexchangeable positions) groups were 94% D and 52% D respectively. In DDM, the required deuteration levels in the dodecyl chain and the maltose sugar head (14 nonexchangeable positions) groups were 89% D and 57% D respectively. Deuterating the detergent molecules directly using hydrothermal reactions was not possible as the harsh conditions of high temperature and pressure were incompatible with the delicate nature of the molecules. The deuteration of methylene units in alkyl hydrocarbons can only be achieved using forced conditions of a hydrothermal catalytic exchange reaction [35], while the deuteration of the sugar groups can be achieved using milder reaction conditions [36]. An alternative approach of deuterating the corresponding sugar molecule and the alkyl chains separately before attaching them together would not be feasible since the sugar groups, glucose and maltose, are reducing sugars, which means they would quickly decompose in the presence of reducing reagents due to the hydrolysis of their hemiacetal moieties. Reducing sugars must be preceded by conversion into glycoside to prevent reduction at the anomeric carbon when exposed to Raney Nickel [36]. Therefore, to achieve specific deuteration levels in the two different parts of any of the two detergent molecules, it was necessary to follow a multiple-step synthesis approach and two sequential deuteration steps. This involved (illustrated in Fig. 2 for OG): **A**) deuterating the alkyl chain at the required deuteration level starting from the corresponding fatty acid and using hydrothermal Pt/C catalysed H/D exchange reactions at 220 °C in the appropriate molar ratio of deuterium and hydrogen atoms in the mixture, reducing the fatty acid molecule to the corresponding alcohol; **B**) attaching the deuterated alcohol to the corresponding acetylated bromo-sugar head group (i.e. 2,3,4,6-tetra-O-acetyl-α-D-glucopyranosyl bromide and 2,3,6,2′,3′,4′,6′-hepta-O-acetyl-a-D-maltosyl bromide) according to standard procedures deacetylation of the sugar head group; **C**) deuterating the sugar head to achieve the required deuteration level by using mild

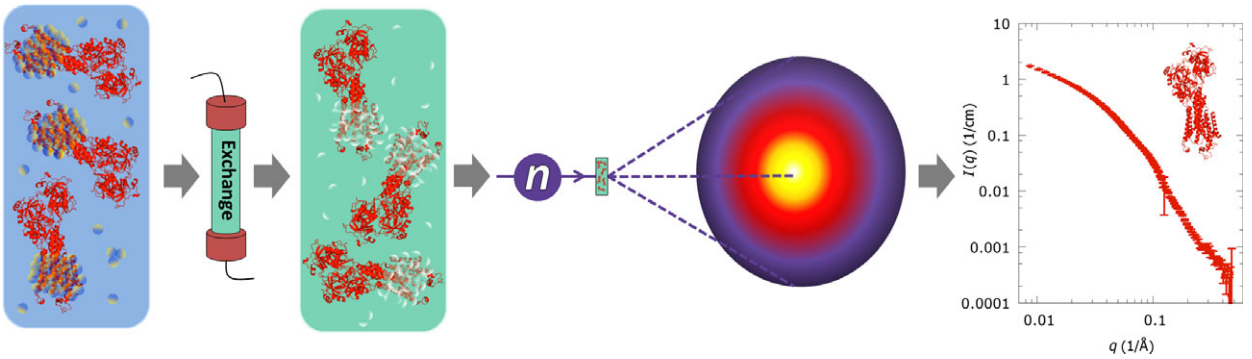

Fig. 1. Process outline of the experiment. Initially, the membrane protein is in H_2O-based buffer and hydrogenated detergents. This sample is then applied to a size exclusion column equilibrated in D_2O-based buffer and the match-out deuterated detergents, allowing the hydrogenated buffer and detergent to be exchanged to their deuterated counterparts. The obtained sample is used directly for SANS measurements to obtain a single contrast dataset yielding only the scattering from the membrane protein. Data from the experiment can then be analysed by generally available software developed for determining the low-resolution structure of proteins in solution.

Table 1. Deuteration levels needed and obtained for *n*-octyl β-D-glucopyranoside (OG) and *n*-dodecyl-β-D-maltopyranoside (DDM).

	OG		DDM	
	Head group	Tail group	Head group	Tail group
Chemical composition of the detergent component	$C_2H_{11}O_6$	C_8H_{17}	$C_{12}H_{21}O_{11}$	$C_{12}H_{25}$
Exchangeable hydrogens	4	0	7	0
Theoretical level of deuteration needed for match-out at 100% D_2O	$C_6D_{7.6}H_{3.4}O_6$	$C_8D_{15.9}H_{1.1}$	$C_{12}D_{15.2}H_{5.8}O_{11}$	$C_{12}D_{22.4}H_{2.6}$
Experimentally obtained level of deuteration in 100% D_2O	$C_6D_{7.64}H_{3.36}O_6$	$C_8D_{15.98}H_{1.12}$	$C_{12}D_{14.98}H_{6.02}O_{11}$	$C_{12}D_{22.25}H_{2.75}$

conditions of Raney Nickel as a catalyst in D_2O/H_2O mixture at 80 °C for 18 h. The latter step allows the incorporation of deuterium atoms on carbons adjacent to free hydroxyl groups (α positions) in the sugar head group with retention of configuration, but it does not affect any H/D back-exchange at the more inert alkyl chain sites [36–38] (see Supporting Information 2 for details).

SANS contrast variation on empty micelles

The deuteration levels obtained from the custom synthesis were close to the desired values (Table 1), implying that the scattering length density from the detergents should theoretically be close to that of 100% D_2O. To experimentally verify this, micelles of the match-out deuterated detergents were measured by SANS in a set of buffers with D_2O content ranging from 60% to 100%. Experiments were performed at ANSTO and FRMII (See SI 4). Background subtracted data are plotted in Fig. 3.

The SANS intensity from both detergents is reduced by more than two orders of magnitude when changing the percentage of D_2O in the buffer from 60% to 100%. Indeed, at 100% D_2O, the signal from the match-out deuterated detergents is effectively at the noise-level over the measured q-range and exhibiting no significant q-dependence. $I(0)$ values (Fig. 3C) were determined by indirect Fourier transformation [39]. The expected parabolic behaviour of the $I(0)$ as a function of D_2O contents was confirmed (Fig. 3C) and the match points were found to be at 102% D_2O for DDM and 103% D_2O for OG.

In Figures 3D and E, the obtained contrast-matched data are compared to previously obtained and published SANS data from the commercially available tail-deuterated counterparts to OG and DDM: d17-OG and d25-DDM [28]. These data, (obtained and plotted with permission from the authors of ref. [28]), are measured at the D22 instrument at ILL, France and plotted at their respective match points which is 90% D_2O for d17-OG and 85% for d-25-DDM [28].

The data from the tail-deuterated detergent d17-OG exhibit the expected q-dependence with an oscillation having a maximum at around 0.15 $Å^{-1}$, but overall a very low intensity of the $I(q)$ at the match-point. Note however, that the d17-OG data had a small experimental discrepancy between the background levels of the measured buffer and sample. Due to the low signal to background ratio, this had a relatively large impact on the obtained scattering intensity as illustrated in Fig 3D which plots both the d17-OG data with background subtracted using the theoretical normalization (light grey curve) and the same data with a small renormalization of the background (dark grey curve). As it is seen, this causes a relatively large shift in the overall scattering intensity, which unfortunately makes a direct quantitative comparison to our data difficult (Fig. 3D). In any case, the density fluctuations expected in the d17-OG are systematic and clearly visible in the $I(q)$-data regardless of the buffer level, while there is no indication of this feature in the data from the match-out deuterated OG.

In the comparison between the d25-DDM at 85% D_2O and the match-out d-DDM at 100% D_2O (Fig. 3E) the above-mentioned experimental discrepancy between the buffer and sample background levels is not present to the same extent. Furthermore, a much stronger difference between the custom synthesized and commercial variants is observed which clearly demonstrates the added value of the custom synthesis of these match-out detergents. Indeed, the scattering intensity of the d25-DDM is 5-6 times as strong around 0.1 $Å^{-1}$ as compared to match-out d-DDM and its q-dependence is, as expected, very significant due to the internal core-shell contrast.

Figure 3F shows the simulated scattering intensity of bR reconstituted in, respectively, a match-out deuterated d-DDM micelle in 100% D_2O and a d25-DDM micelle at 85% D_2O. Note that, for d25-DDM, the overall scattering intensity is lower than for d-DDM. This is a trivial consequence of the different D_2O concentrations. More importantly, the q-dependence differs significantly in the two systems.

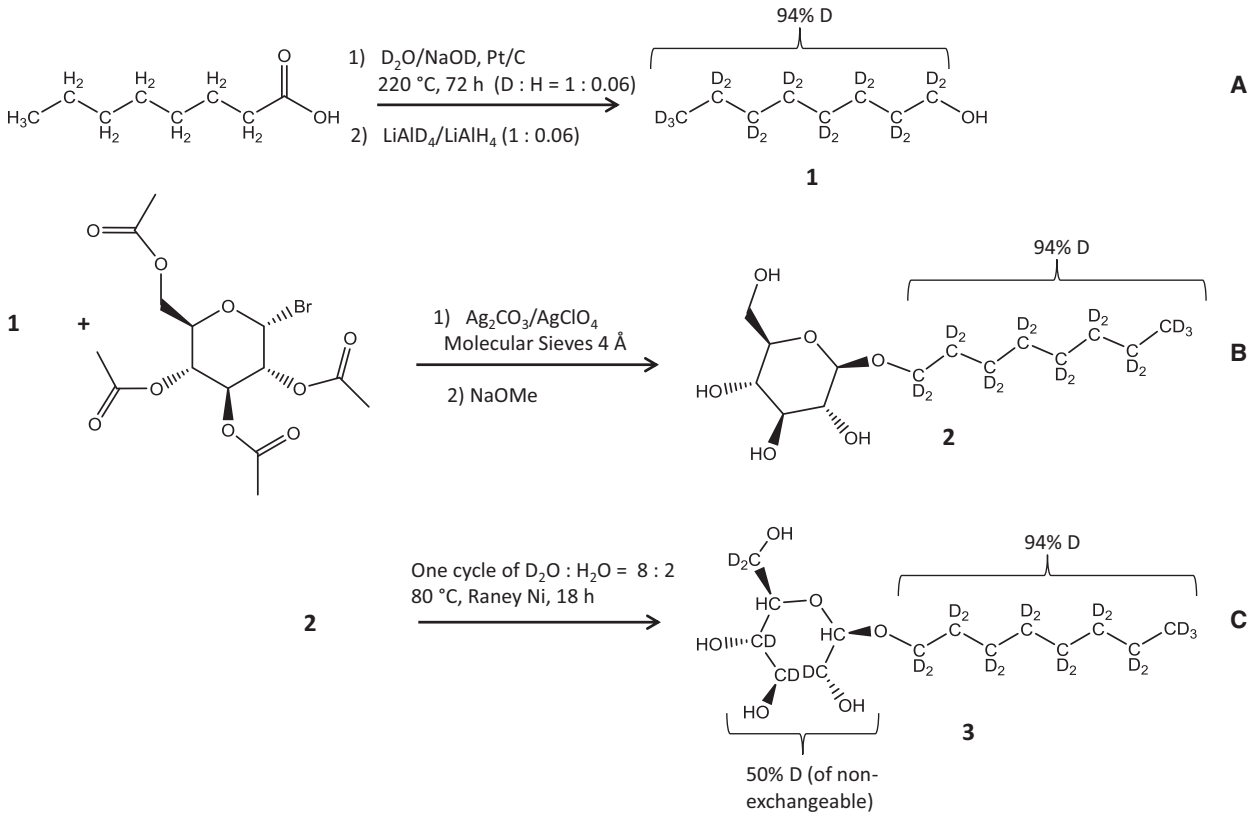

Fig. 2. Reaction scheme for the synthesis of specifically deuterated levels of OG (the corresponding scheme for DDM can be found in Fig. S1). Step (A) The fatty acid is deuterated by Pt/C catalysed H/D exchange reactions at 220 °C to produce the correctly deuterated version and then it is reduced to the corresponding alcohol (1) using the specified D:H ratio. Step (B) The deuterated alcohol (1) is coupled with the acetylated bromo-sugar head group, producing the tail-deuterated version of the detergent, which is then deacetylated to produce (2). Step (C) The sugar head group is deuterated via Raney Nickel catalysis to produce the final partially deuterated detergent (3) with different levels of deuteration in the head and the tail groups.

The oscillation around 0.1 Å^{-1} arising from the core-shell contrast of the d25-DDM is still visible in the bR-micelle complex, but already from $q > 0.02$ Å^{-1} the two $I(q)$-functions start differing (see dashed line in Fig. 3F) as a result of the internal contrast of the d25-DDM micelles. This is already visible in the Guinier range and show that not even a reliable value for the R_g of bR can be obtained with the d25-DDM as reconstitution system. Similar effects, although less pronounced are to be expected if using d17-OG as the reconstitution system.

Exchange of protonated to deuterated detergents

The extent of exchange from hydrogenated to deuterated detergents in samples of membrane proteins outlined in Fig. 1, was evaluated by monitoring the background SANS signal at high q as a function of SEC flowrate, as the hydrogen from any nonexchanged buffer or detergent would generate an increase in incoherent background scattering. In initial experiments, the background scattering was found to be very high due to incomplete exchange of the detergent. The Agilent Bio SEC-3-300 column, used in combination with a high flowrate (0.7 $\text{mL}\cdot\text{min}^{-1}$) was found to be the cause and by lowering the flowrate to 0.4 $\text{mL}\cdot\text{min}^{-1}$ the problem was solved. Hence, for this method to perform as intended, it is of paramount importance to use a sufficiently low flowrate in the SEC to enable an enhanced H/D exchange of detergent and solvent (see further details in Supporting Information 3).

Membrane protein data and analysis

To evaluate this method, five structurally different membrane proteins were investigated; bacteriorhodopsin (bR), maltoporin (LamB), photosystem I (PSI), the ionotropic glutamate receptor A2 (GluA2) and the sarco/endoplasmatic reticulum Ca^{2+} ATPase

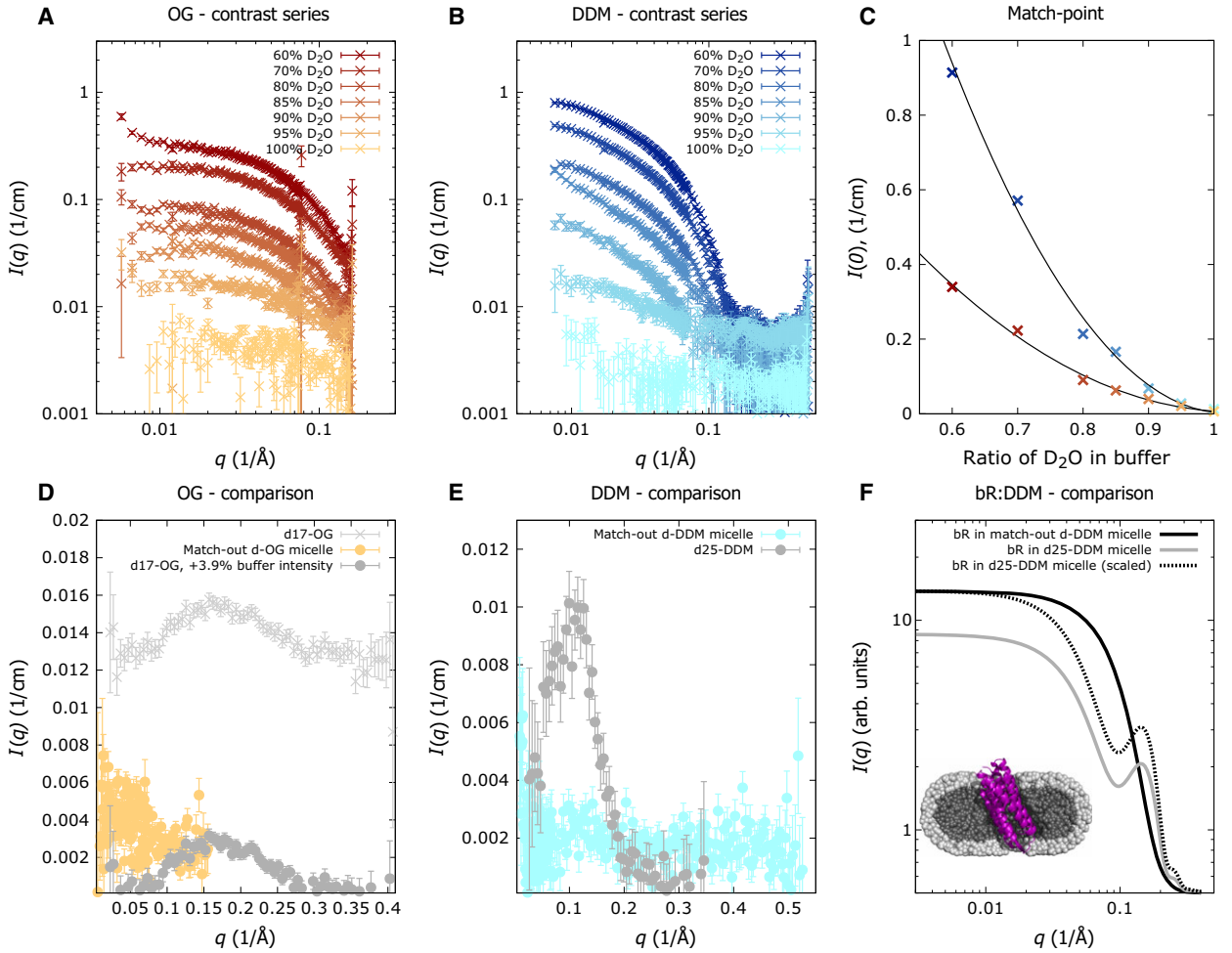

Fig. 3. (A) Background subtracted SANS data from match-out deuterated OG in increasing percentage of D_2O in the buffer. (B) SANS data from match-out deuterated DDM in increasing percentage of D_2O in the buffer. (C) Experimental I(0) values plotted (points) and the corresponding quadratic power law fits (lines). (D) Comparison of I(q) from match-out d-OG (yellow) and d17-OG (light and dark grey), both measured at their match point. Light grey curve plots d17-OG with the usual background subtraction. In the dark grey curve, the d17-OG background has been empirically increased by a factor of 1.039. (E) Comparison of match-out d-DDM (turquoise) and d25-DDM (grey) measured at its match point. Data from d17-OG and d25-DDM are reproduced from [28]. (A)-(E) Error bars are the standard deviation (SD), obtained from counting statistics and standard error propagation. (F) Simulation of a Bacteriorhodopsin monomer measured by SANS, respectively, in match-out d-DDM (black) and in d25-DDM (grey and dashed) micelles.

(SERCA). The first three proteins, bR, LamB and PSI, are all examples of membrane proteins that have either no or small domains outside the cell membrane. These three proteins were also chosen as they are relatively stable and at the same time representative of the wide range of molecular weights found in membrane proteins viz. ~ 27 kDa (bR), ~ 47 kDa (LamB) and ~ 650 kDa (PSI). Two additional membrane proteins, GluA2 (~ 385 kDa) and SERCA (~ 110 kDa), were selected as examples of more unstable membrane

Fig. 4. Experimental SANS data (coloured points) and the resulting model fits (black full and dashed lines) for the five investigated membrane proteins. Error bars are the standard deviation (SD), obtained from counting statistics and standard error propagation. Note that instrumental resolution effects are included in the models, which then exhibit small discontinuities at medium *q*-values. Inserts: The corresponding pair-distance distribution functions as determined by Indirect Fourier transform [39] with identical colour scheme. Figures are the known structures from crystallography together with the *ab initio* bead models where appropriate. Note that SERCA (data, model and *p (r)*) contain a fraction of aggregated protein.

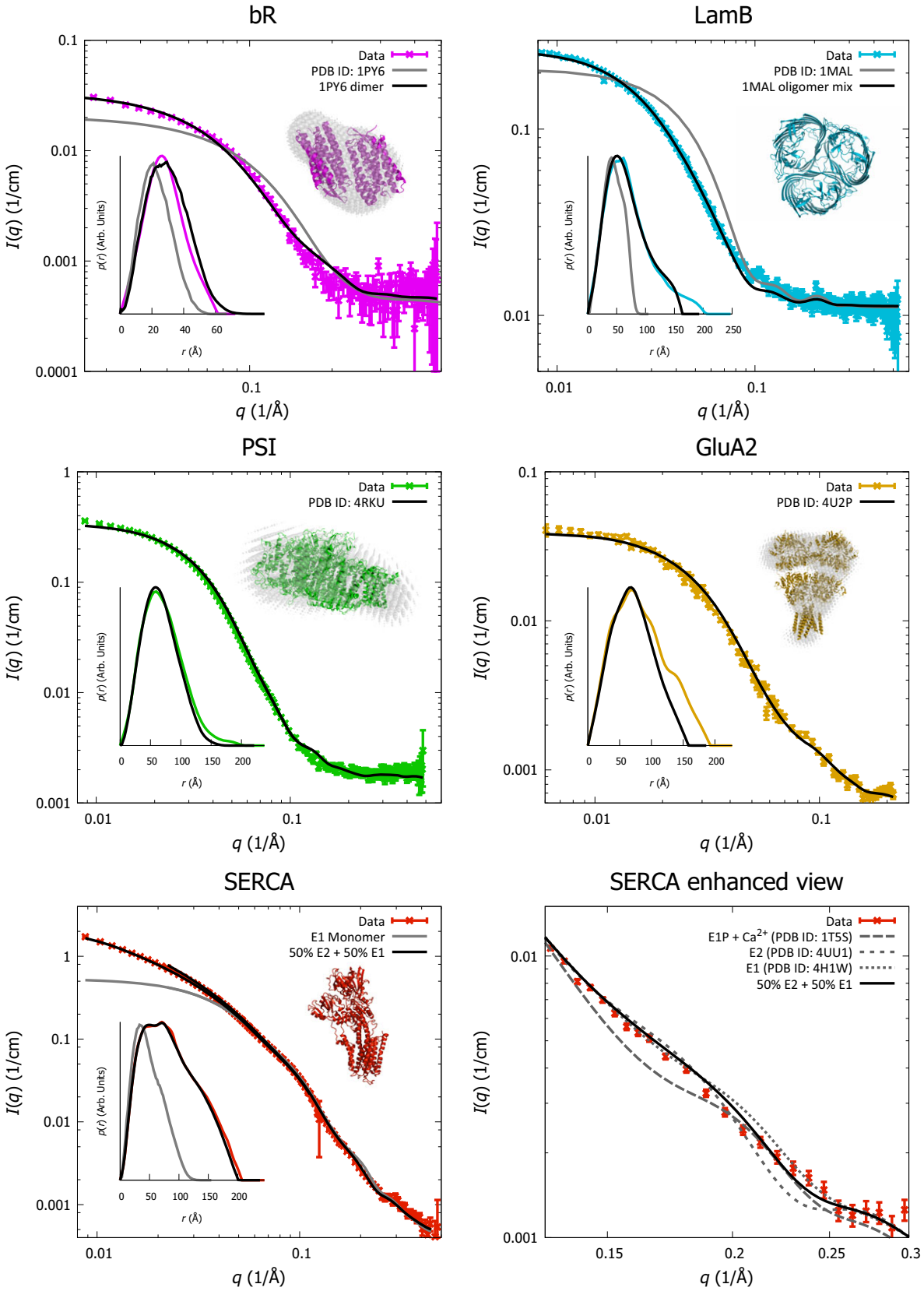
bR
Data
PDB ID: 1PY6
1PY6 dimer
I(q) (1/cm)
p(r) (Arb. Units)
r (Å)
q (1/Å)
LamB
Data
PDB ID: 1MAL
1MAL oligomer mix
PSI
Data
PDB ID: 4RKU
GluA2
Data
PDB ID: 4U2P
SERCA
Data
E1 Monomer
50% E2 + 50% E1
SERCA enhanced view
Data
E1P + Ca2+ (PDB ID: 1T5S)
E2 (PDB ID: 4UU1)
E1 (PDB ID: 4H1W)
50% E2 + 50% E1

proteins with complex structures and large protein domains outside the membrane spanning region that may be captured in distinct functional states. SANS data on the LamB protein were obtained on the QUOKKA instrument at ANSTO, GluA2 was measured on KWS1 at FRM II and data from bR, PSI and SERCA were obtained on the D22 instrument at ILL. The SANS data and results obtained using the invisible detergents in 100% D_2O are presented in Fig. 4 (See Supporting Information 4 for further details).

Crystal structures were available for all proteins, and these were used as a basis for modelling the theoretical scattering patterns to be compared to the experimental data (Fig. 4). bR was found to agree with a dimer structure, LamB, with a combination of homotrimers and higher oligomers of these, PSI data with a monomer structure, GluA2 with a homotetramer and SERCA with a combination of two structural states combined with a minor aggregated fraction of SERCA using a previously developed approach [40] (see SI 4 for more details). Hydration layers were added to all water-exposed surfaces. Instrumental resolution effects on the SANS data were taken into account in the analysis [41] and the required values for the $\Delta q(q)$ for the resolution function calculations for the different instrumental settings were provided by the beamlines. The resolution effect is most clearly visible for the SERCA data where an (expected) discontinuity of the fitted model is observed around $q = 0.03$ 1/Å for all data. A constant background and a scale factor were fitted to obtain the best agreement between the data and model, shown in Fig. 4. The figure also plots the theoretical pair distance distribution functions $p(r)$ calculated from the fitted models together with the ones obtained from the data by indirect Fourier transformation [39]. The values of radius of gyration, R_g, and maximum internal distances, D_{max}, obtained from the $p(r)$ functions, are listed in Table 2 together with molecular masses estimated from the estimated Porod volume and the partial specific molecular volume found by Mylonas *et al.* [42]. Table 2 compares these values to the theoretical R_g, D_{max} and MW values based on the available crystal structures. Note that the experimental estimates for the Porod volume are not expected to have a precision better than ±20% [30]. Finally, *Ab initio* bead modelling was performed for bR, PSI and GluA2 and compared with the known structures (See Fig. 4 and SI 4).

Bacteriorhodopsin with a monomeric molecular weight of ~ 27 kDa, is a relatively small membrane protein with seven transmembrane helices. Due to its small size, it scatters weakly and any interfering signal from the detergent should be visible in the data. As it is evident from Fig. 4, the experimental data correspond well with a dimer of bR (PDB ID: 1PY6). While bR is traditionally found as a monomer or trimer, a dimeric form is well documented [43]. A closer look into the structural parameters in Table 2, show that the experimentally obtained R_g, D_{max} and MW values are in most cases slightly larger than what would be expected from the crystal structures of the dimer. This larger size is not only indicated in the obtained *ab initio* structure (Fig. 4) and can both be indications of slightly more loose or open dimer structures in solution than in the crystals but may also indicate the presence of small populations of higher order oligomers. These questions could be pursued further in a future work. However, the ability to discern the oligomeric state shows that the method can probe the structure of relatively small membrane proteins in solution without any significant contribution from the match-out deuterated detergent. bR has the same size and general fold as many G protein-coupled receptors (GPCRs) [44]. The data show that this interesting class of membrane proteins, typically too small for cryo-EM fall well within the range of this SANS-based method.

The LamB protein is a homotrimeric beta barrel porin structure with a monomer weight of ~ 142 kDa [45], hence a membrane protein with intermediate molecular weight. The SANS data presented in Fig. 4 were found to agree with an oligomeric mixture of monomeric, trimeric and heptameric states of the

Table 2. Structural parameters deduced from the experimental data and the calculated theoretical values from the fitted models as obtained through Indirect Fourier Transform. R_g: Radius of gyration. D_{max}: Maximum distance present in the scattering particle. MW: Molecular weight. Experimental values obtained from SANS data, theoretical values calculated from the available crystal structures.

	R_g exp. [Å]	R_g theo. [Å]	D_{max} exp. [Å]	D_{max} theo. [Å]	*MW exp. [kDa]*	*MW calc. [kDa]*
bR	21.6 ± 0.04	17.4	60.2 ± 0.9	53	44.6	27*2
LamB	57.9 ± 0.2	33.4	201 ± 1	87	210	47*3
PSI	55.2 ± 0.2	51.3	199 ± 5	159	473	650
GluA2	60.0 ± 0.4	56.2	166 ± 1	173	278	385
SERCA E1 + E2	56.4 ± 0.1	38.4	204.5 ± 0.6	123	460	110

underlying LamB homotrimer (PDB ID: 1MAL, See SI 4 for further details), making an *ab initio* structure irrelevant. While it is clear from the data and the values for R_g, D_{max} and MW listed in Table 2 that the data must arise from, on average, larger particles than the basic LamB homotrimeric structure, another base set of structures derived from the homo-trimer could likely also have provided a good representation of the measured data. A small deviation between the model and data is visible at 0.11 $Å^{-1}$, this hints towards the possibility of investigating finer structural details of the LamB oligomerization with this method. However, a larger set of data would be required for this purpose.

Plant PSI is a large protein complex with a diameter of around 20 nm that comprises multiple, mostly alpha-helical subunits [46,47]. It is evident from the SANS data in Fig. 4 that the overall structure of PSI in solution is highly similar to the one recently found by X-ray crystallography (PDB ID: 4RKU). Interestingly, a small discrepancy is found around 0.1 $Å^{-1}$ and the experimental values for R_g and D_{max} are slightly higher than the comparable value for the crystal structure. The slightly larger size observed by SANS is also reflected in the plotted *ab initio* structure (Fig. 4). The observed differences likely stem from the fact that ~ 10% of the amino acid residues are not found in the crystal structure. Other contributing factors could be that the solution structure, due to increased flexibility, is slightly different from the one confined in the crystal or that the crystal structure is from pea PSI and the SANS data were obtained from barley PSI. In either case, it is interesting that this method is able to demonstrate minor discrepancies between the known model and the obtained SANS data for this otherwise highly studied membrane protein complex.

Ionotropic glutamate receptor A2 is a neurotransmitter-activated receptor with a structure consisting of a large, extended homotetramer [48]. The scattering data correspond very well with the known structure of GluA2 (PDB ID: 4U2P), which is also seen from the resemblance between the crystal structure and the *ab inito* model (see Fig. 4) and from the good agreement (within the experimental accuracy) between the experimental and expected values for the R_g, D_{max} and MW listed in Table 2. The values found in Table 2 also indicate a good agreement with the expected structure within the expected accuracy. This demonstrates that the method can readily probe the structure of large and complicated membrane proteins and, in this case, confirm that the crystal structure is representative of the solution structure.

Sarco/endoplasmatic reticulum Ca^{2+} ATPase is a calcium-transporting ATPase and more difficult to stabilize in solution than the other proteins in this study. It has a complex fold with three major cytoplasmic domains outside the membrane spanning region that rearrange with respect to each other during the calcium transport cycle [49]. Several of the structural states relating to the pumping cycle of SERCA have been revealed by crystallography via stabilization with cofactors and inhibitors [50]. However, some states and dynamic transitions are still debated. Here, the structure in the absence of calcium and stabilized by the nonhydrolysable ATP analogue AMPPCP has been investigated, representing the so-called E1 and E2 states. High-quality SANS data have been collected as evidenced by the relatively small error bars and the presence of significant features in the high-q region. The data correspond to monomeric SERCA together with a minor fraction of oligomeric SERCA (~ 2% of the molecules, see SI 4 for details). The data clearly delineate calcium-free SERCA structures, as is also evident from the enhanced view in Fig. 4 where the structure with calcium (PDB ID: 1T5S) completely fails to describe the finer details observed in the experimental data. The structural state probed in this study is expected to be dynamic and potentially switch between the E2 (PDB ID: 4UU1) and E1 (PDB ID:4H1W) calcium-free states [50]. Fitting the individual E2 and E1 states and a superposition of the two structures to the data indeed reveals that while both the calcium-free states represent the features in the data better than the calcium-bound form, the best description of the data is obtained by a linear combination of the E2 and E1 states with a distribution of 50% E2 and 50% E1 (see SI 4 for details). Not only does this confirm what has been previously suggested in the literature but it also provides a result that could not have been obtained using a traditional crystallographic approach. Additionally, this result demonstrates that the workflow and method presented here is compatible with probing the finer structure of this challenging and unstable type of membrane proteins. There was aggregation in a fraction of the SERCA sample, as clearly seen from the experimental data in Fig. 4, and reflected in the R_g, D_{max} and MW listed in Table 2. This effect was included in the modelling as a structure factor for fractal aggregates and using a previously developed approach [40]. However, since the two structures of interest, E1 and E2, had approximately the same size, and hence the same scattering intensity at low-q, the aggregation did not affect the assessment of the equilibrium between these states. A detailed description of the data analysis, the structure

factor as well as a more thorough discussion of this matter can be found in the supplemental information (SI 4).

Discussion

The feasibility of using custom-synthesized match-out deuterated detergents for elucidating the structure of membrane proteins by solution SANS has been demonstrated. Firstly, the synthesis of partly deuterated versions of DDM and OG were developed and the desired match-out deuteration confirmed by SANS. Secondly, the detergents were successfully used for stabilizing membrane proteins while performing SANS experiments. Thirdly, by analysis of the obtained SANS data, it was demonstrated that this method does indeed perform as well as expected and hence provides a novel and easy-to-use tool for low-resolution structural studies of membrane proteins.

For the past decade, performing a SAXS experiment to complement high-resolution structural work by crystallography has become a standard approach when investigating soluble proteins [51]. This is not least due to the easy analysis made possible by the ATSAS suite [30] and development of stable and high-throughput SAXS beamlines [52]. This approach is now directly transferable to membrane proteins by using the approach of deuterated detergents and SANS.

The method of using match-out deuterated detergents to obtain solution structures of membrane proteins fills an important gap in the toolbox for their detailed investigation. While traditional protein crystallography has undeniably produced fantastic new insights into biological processes over several decades, obtaining crystals of membrane proteins diffracting to high resolution remains a bottleneck [53]. Indeed, larger flexible membrane proteins are under-represented in the protein data bank due to this obstacle. The method presented here allows for probing the structure in detail early in the process when a robust expression and purification protocol has been established. Recent advances in both the methodology and hardware have matured Cryo-EM to a technique that has become a major game changer in structural biology [8]. However, a major drawback of Cryo-EM is the requirement of proteins with a molecular mass above ~ 100-150 kDa to obtain sufficiently high signal-to-noise ratios to allow for the alignment and averaging of the individual frames required for obtaining the desired high-resolution data [8]. This means that many important membrane proteins are too small for Cryo-EM (although use of the Volta Phase Plate shows great promise for cryo-EM studies of even smaller proteins [54]). NMR spectroscopy is also a popular method for determining the high-resolution structure of membrane proteins [55], but due to the overcrowding of the spectra, only relatively small proteins (~ 20-30 kDa) may be solved. Hence, the combined SANS and invisible detergent method described in this paper provides an easily applicable alternative that allows for analysing protein structures with a resolution down to about 10 Å, and that importantly contributes to bridging the gap between existing methods.

Several other strategies have been proposed in the literature which utilize some of the aspects of the method presented here. The use of small-angle X-ray scattering (SAXS) for elucidating the structure of membrane proteins in detergent micelles has been thoroughly tested [56–59] but thus far mainly revealed information on the detergent rim around the membrane proteins. Furthermore, using so-called nanodiscs coupled with small-angle scattering has also been shown to be possible but the sample preparation remains challenging [11,60]. This is contrasted with the approach presented here, where the sample preparation is uncomplicated and the signal almost exclusively comes from the membrane protein, significantly simplifying the data analysis and increasing the information that can be extracted about the structure of the investigated membrane protein. Importantly, this method allows for probing the structure of uncrystalizable dynamic structural states of proteins. Recent technical developments in SEC-SANS sample environments will furthermore allow for performing the whole workflow outlined in Fig. 1 *in situ* at the neutron instrument, together with removing any oligomeric species caused by unstable proteins [61].

Five different membrane proteins and two detergents were investigated in this study. The data demonstrate the general applicability of the approach and provide promising perspectives for future use. The basic idea of match-out deuteration may easily be generalized to other detergent types to accommodate special needs for particular membrane proteins or in combination with selective deuteration of different subunits.

Methods

General materials

Hydrogenated Octyl-β-D-glucopyranoside (OG) was purchased from Applichem while hydrogenated n-dodecyl-β-D-maltopyranoside (DDM) was purchased from Sigma Aldrich. Match-out deuterated detergents were custom

synthesized as described briefly below and in detail in the supplemental information. The membrane proteins used in the present study were expressed and purified according to standard protocols as described in the supplemental information. All pH values have been measured using a standard glass electrode and all reported values are from the direct measurement [62].

Densitometry

Densitometry was performed using a DMA 5000 density meter (Anton Paar). Octyl-β-D-glucopyranoside (OG) (Sigma-Aldrich) was solubilized in 20 mM Tris/HCl, pH 7.5 and 100 mM NaCl in concentrations of 25 and 100 mM. n-dodecyl-β-D-maltopyranoside (DDM) (Sigma-Aldrich) was solubilized in identical buffer at concentrations of 15 and 60 mM. All samples were prepared in triplicates and measured at 4 °C intervals between 4 °C and 28 °C. See further details in the supplemental information.

General detergent synthesis

Chemicals and reagents of the highest grade were purchased from Sigma-Aldrich and Carbosynth Limited (Berkshire, UK) and were used without further purification. Solvents were purchased from Sigma-Aldrich and Merck and were purified by established methods [63]. NMR solvents were purchased from Cambridge Isotope Laboratories Inc. and Sigma-Aldrich and were used without further purification. D_2O (99.8%) was supplied by Sigma-Aldrich. Thin layer chromatography (TLC) was performed on Fluka Analytical silica gel aluminium sheets (25 F254). Davisil® silica gel (LC60Å 40-63 micron) was used for bench-top column chromatography.

Deuteration of octanoic acid and dodecanoic acid was performed using hydrothermal H/D exchange reactions in D_2O at 220 °C by mixing the appropriate amount of fatty acid with NaOD and Pt/C (10% w/w) in a Mini Benchtop 4560 Parr Reactor (600 mL vessel capacity, 3000 psi maximum pressure, 350 °C maximum temperature). This was followed by filtering the catalyst, acidifying the solution and then extracting the aqueous phase with ethyl acetate. Thin layer chromatography was used (referenced with the protonated compound) to estimate the purity and to develop separation protocols. ^{1}H NMR (400 MHz), ^{13}C NMR (100.6 MHz) and ^{2}H NMR (61.4 MHz) spectra were recorded on a Bruker 400 MHz spectrometer at 298 K. Chemical shifts, in p.p.m., were referenced to the residual signal of the corresponding NMR solvent. Deuterium NMR was performed using the probe's lock channel for direct observation. Electrospray ionization mass spectra (ESI-MS) were recorded on a 4000 QTrap AB Sciex spectrometer. The overall percentage deuteration of the molecules was calculated by MS using the isotope distribution analysis of the different isotopologues. This was calculated taking into consideration the ^{13}C natural abundance, whose contribution was subtracted from the peak area of each M + 1 isotopologue to allow for accurate estimation of the percentage deuteration of each isotopologue.

Transfer of membrane proteins into deuterated detergents

The transfer was performed using an Agilent Bio SEC-3-300 column with a flowrate of 0.4 mL·min^{-1}. The flow through from the column was collected, measured and used for background subtraction.

Buffers used for PSI, GluA2 and bR contained 0.5 mM match-out deuterated DDM, 20 mM Tris/DCl pH 7.5 and 100 mM NaCl in D_2O. For LamB, 40 mM match-out deuterated OG was used instead of DDM. For SERCA, the buffer used consisted of 20 mM MOPS pH 6.8, 100 mM KCl and 0.5 mM DDM.

SANS measurements

The SANS measurements of the deuterated OG were performed at KWS 1, Forschungs Neutronenquelle Heinz Maier-Leibnitz, Munich (FRM II). A neutron wavelength of 4.5 Å (±10% FWHM) was used at two sample-to-detector distances covering q-ranges of 0.012–0.16 Å^{-1} and 0.0057–0.077 Å^{-1}. Precalibrated plexiglass was used as a standard for absolute calibration of the scattered intensity $I(q)$ in units of 1/cm, where $q = (4\pi/\lambda)\sin(\theta)$ and 2θ is the scattering angle and λ is the wavelength. GluA2 was measured at the same instrument using three sample-to-detector distances: 1.5 m and 4.0 m with 4 m collimation and 8.0 m with 8 m collimation were used.

The SANS measurements of the LamB protein in deuterated OG and empty deuterated DDM micelles were performed at QUOKKA [64], Australian Nuclear Science and Technology Organization (ANSTO), Sydney. A neutron wavelength of 5.0 Å (±10% FWHM) was used at two sample-to-detector distances, covering q-ranges of 0.017–0.51 Å^{-1} and 0.0076–0.098 Å^{-1}. Data were absolutely calibrated by an attenuated direct beam transmission measurement of the scattered intensity.

The SANS measurements of the bR, SERCA and PSI in deuterated DDM were performed at D22, Institut Laue-Langevin (ILL), Grenoble. A neutron wavelength of 6.0 Å (±10% FWHM) was used at two sample-to-detector distances covering q-ranges of 0.022–0.48 Å^{-1} and 0.0087–0.12 Å^{-1}. H_2O was used as a standard for absolute calibration of the scattered intensity.

SANS data analysis

Pair distance distribution functions, $p(r)$ and the associated values for the radius of gyration, R_g, and maximum particle diameter, D_{max}, were obtained from the scattering data using

a Bayesian indirect Fourier transform [39]. Porod volume-based values for the protein molar mass were estimated by the GNOM program of the ATSAS package [65]. *Ab initio* models of the proteins were obtained using the DAMMIF program of the ATSAS package [65]. Theoretical scattering patterns for the relevant protein structures were calculated using the program WillItFit [31]. Hydrogen and deuterium was added to the structures by the Phenix program Ready-Set! [66], exchanging all labile hydrogens for deuterium. A surface hydration layer was added to the hydrophilic areas of the structures using an in-house routine which identifies surface residues and places beads at a distance of 5 Å from the C_α of the surface residues. This routine allows for not adding a water layer at the hydrophobic portion of the protein surface as identified by the Orientations of proteins in Membranes' database (OPM) [67].

Acknowledgements

The authors acknowledge Dr. Robert Knott at ANSTO and Dr. Adam Round at ESRF for their assistance in obtaining supporting SAXS data. We thank ANSTO, ILL and FRM II for awarding us beamtime for this project at, respectively, the QUOKKA, D22 and KWS-1 instruments. RV, CK, TST, JJD and JSK thank Eric Gouaux for providing the GluA2cryst construct and protein purification protocol. Dr. Frank Gabel and Dr. Christine Ebel are thanked for kindly providing data on the tail-deuterated detergents previously published in [28]. PhD student Nicolai Tidemand Johansen is thanked for helping with the SANS measurements of GluA2. We thank the Danish Agency for Science, Technology and Innovation funding agency for making this study possible through a Sapere Aude grant to LA. RV, CK, and JSK acknowledge the support from the Lundbeck Foundation, The Danish Council for Independent Research – Medical Sciences and GluTarget. The authors also acknowledge financial support from the Center for Synthetic Biology (bioSYNergy) funded by the UCPH Excellence Programme for Interdisciplinary Research and to the Lundbeck foundation "BRAINSTRUC" project. The National Deuteration Facility is partly supported by the National Collaborative Research Infrastructure Strategy – an initiative of the Australian Government.

Author contributions

SRM, TD and LA conceived the project. TD developed methods and synthesized the deuterated detergents. SRM, AJZN, PEJ, MB, CO, PN, RV, TST, JJD, CK and JSK produced and provided proteins. SRM, MCP, SARK, PH, and AHL performed the experiments. AHL, NSG, GVJ, MCP and SARK performed the data analysis. HF, EG and AM were responsible for the SANS instrument and participated in the SANS measurements. SRM, TD and LA cowrote the paper.

Conflict of interest

The authors declare no competing financial interests.

References

1 Loll PJ (2014) Membrane proteins, detergents and crystals: what is the state of the art? *Acta Crystallogr Sect F Struct Biol Commun* **70**, 1576–1583.
2 Diller A, Loudet C, Aussenac F, Raffard G, Fournier S, Laguerre M, Grélard A, Opella SJ, Marassi FM & Dufourc EJ (2009) Bicelles: a natural "molecular goniometer" for structural, dynamical and topological studies of molecules in membranes. *Biochimie* **91**, 744–751.
3 Poulos S, Morgan JLW, Zimmer J & Faham S (2015) Bicelles coming of age. In *Membrane Proteins Engineering, Purification and Crystallization* 1st edn. pp. 393–416. Elsevier Inc., Amsterdam.
4 Midtgaard SR, Pedersen MC, Kirkensgaard JJK, Sørensen KK, Mortensen K, Jensen KJ & Arleth L (2014) Self-assembling peptides form nanodiscs that stabilize membrane proteins. *Soft Matter* **10**, 738–752.
5 Knowles TJ, Finka R, Smith C, Lin Y-P, Dafforn T & Overduin M (2009) Membrane proteins solubilized intact in lipid containing nanoparticles bounded by styrene maleic acid copolymer. *J Am Chem Soc* **131**, 7484–7485.
6 Popot J-L, Althoff T, Bagnard D, Banères J-L, Bazzacco P, Billon-Denis E, Catoire LJ, Champeil P, Charvolin D, Cocco MJ *et al.* (2011) Amphipols from A to Z. *Annu Rev Biophys* **40**, 379–408.
7 Ritchie TK, Grinkova YV, Bayburt TH, Denisov IG, Zolnerciks JK, Atkins WM & Sligar SG (2009) Chapter 11 reconstitution of membrane proteins in phospholipid bilayer nanodiscs. *Methods Enzymol* **464**, 211–231.
8 Nogales E & Scheres SHW (2015) Cryo-EM: a unique tool for the visualization of macromolecular complexity. *Mol Cell* **58**, 677–689.
9 Murray DT, Das N & Cross TA (2013) Solid state NMR strategy for characterizing native membrane protein structures. *Acc Chem Res* **46**, 2172–2181.
10 Maric S, Skar-Gislinge N, Midtgaard S, Thygesen MB, Schiller J, Frielinghaus H, Moulin M, Haertlein M, Forsyth VT, Pomorski TG *et al.* (2014) Stealth carriers for low-resolution structure determination of membrane

proteins in solution. *Acta Crystallogr D Biol Crystallogr* **70**, 317–328.
11 Kynde SAR, Skar-Gislinge N, Pedersen MC, Midtgaard SR, Simonsen JB, Schweins R, Mortensen K & Arleth L (2014) Small-angle scattering gives direct structural information about a membrane protein inside a lipid environment. *Acta Crystallogr D Biol Crystallogr* **70**, 371–383.
12 Skar-Gislinge N, Kynde SAR, Denisov IG, Ye X, Lenov I, Sligar SG & Arleth L (2015) Small-angle scattering determination of the shape and localization of human cytochrome P450 embedded in a phospholipid nanodisc environment. *Acta Crystallogr Sect D Biol Crystallogr* **71**, 2412–2421.
13 Nawroth T, Dose K & Conrad H (1989) Neutron small angle scattering of detergent solubilized and membrane bound ATP-synthase. *Phys B Condens Matter* **156–157**, 489–492.
14 Sverzhinsky A, Qian S, Yang L, Allaire M, Moraes I, Ma D, Chung JW, Zoonens M, Popot JL & Coulton JW (2014) Amphipol-trapped ExbB-ExbD membrane protein complex from escherichia coli: a biochemical and structural case study. *J Membr Biol* **247**, 1005–1018.
15 Wise DS, Karlin A & Schoenborn BP (1979) An analysis by low-angle neutron scattering of the structure of the acetylcholine receptor from Torpedo californica in detergent solution. *Biophys J* **28**, 473–496.
16 Le RK, Harris BJ, Iwuchukwu IJ, Bruce BD, Cheng X, Qian S, Heller WT, O'Neill H & Frymier PD (2014) Analysis of the solution structure of Thermosynechococcus elongatus photosystem i in n-dodecyl-β-d-maltoside using small-angle neutron scattering and molecular dynamics simulation. *Arch Biochem Biophys* **550–551**, 50–57.
17 Hunt JF, McCrea PD, Zaccaï G & Engelman DM (1997) Assessment of the aggregation state of integral membrane proteins in reconstituted phospholipid vesicles using small angle neutron scattering. *J Mol Biol* **273**, 1004–1019.
18 Wang ZY, Muraoka Y, Nagao M, Shibayama M, Kobayashi M & Nozawa T (2003) Determination of the B820 subunit size of a bacterial core light-harvesting complex by small-angle neutron scattering. *Biochemistry* **42**, 11555–11560.
19 Gall A, Dellerue S, Lapouge K, Robert B & Le L (2001) Scattering measurements on the membrane protein subunit B777 in a detergent. *Biopolymers* **58**, 231–234.
20 Cardoso MB, Smolensky D, Heller WT & O'Neill H (2009) Insight into the structure of light-harvesting complex II and its stabilization in detergent solution. *J Phys Chem B* **113**, 16377–16383.
21 Clifton LA, Johnson CL, Solovyova AS, Callow P, Weiss KL, Ridley H, Le Brun AP, Kinane CJ, Webster JRP, Holt SA *et al.* (2012) Low resolution structure and dynamics of a colicin-receptor complex determined by neutron scattering. *J Biol Chem* **287**, 337–346.
22 Pachence JM, Edelman IS & Schoenborn BP (1987) Low-angle neutron scattering analysis of Na/K-ATPase in detergent solution. *J Biol Chem* **262**, 702–709.
23 Perkins SJ & Weiss H (1983) Low-resolution structural studies of mitochondrial ubiquinol:cytochrome c reductase in detergent solutions by neutron scattering. *J Mol Biol* **168**, 847–866.
24 Gabel F, Lensink MF, Clantin B, Jacob-Dubuisson F, Villeret V & Ebel C (2014) Probing the conformation of FhaC with small-angle neutron scattering and molecular modeling. *Biophys J* **107**, 185–196.
25 Block MR, Zaccaï G, Lauquin GJ & Vignais PV (1982) Small angle neutron scattering of the mitochondrial ADP/ATP carrier protein in detergent. *Biochem Biophys Res Commun* **109**, 471–477.
26 Osborne HB, Sardet C, Michel-Villaz M & Chabre M (1978) Structural study of rhodopsin in detergent micelles by small-angle neutron scattering. *J Mol Biol* **123**, 177–206.
27 Nogales A, García C, Pérez J, Callow P, Ezquerra TA & González-Rodríguez J (2010) Three-dimensional model of human platelet integrin alphaIIb beta3 in solution obtained by small angle neutron scattering. *J Biol Chem* **285**, 1023–1031.
28 Breyton C, Gabel F, Lethier M, Flayhan A, Durand G, Jault J-M, Juillan-Binard C, Imbert L, Moulin M, Ravaud S *et al.* (2013) Small angle neutron scattering for the study of solubilised membrane proteins. *Eur Phys J E Soft Matter* **36**, 71.
29 Breyton C, Flayhan A, Gabel F, Lethier M, Durand G, Boulanger P, Chami M & Ebel C (2013) Assessing the conformational changes of pb5, the receptor-binding protein of phage T5, upon binding to its escherichia coli receptor FhuA. *J Biol Chem* **288**, 30763–30772.
30 Petoukhov MV, Franke D, Shkumatov AV, Tria G, Kikhney AG, Gajda M, Gorba C, Mertens HDT, Konarev PV & Svergun DI (2012) New developments in the ATSAS program package for small-angle scattering data analysis. *J Appl Crystallogr* **45**, 342–350.
31 Pedersen MC, Arleth L & Mortensen K (2013) WillItFit: a framework for fitting of constrained models to small-angle scattering data. *J Appl Crystallogr* **46**, 1894–1898.
32 Curtis JE & Krueger S. SASSIE. NIST.
33 Ilavsky J & Jemian PR (2009) Irena: tool suite for modeling and analysis of small-angle scattering. *J Appl Crystallogr* **42**, 347–353.
34 Schneidman-Duhovny D, Hammel M & Sali A (2010) FoXS: a web server for rapid computation and fitting of SAXS profiles. *Nucleic Acids Res* **38**, 540–544.

35 Darwish TA, Luks E, Moraes G, Yepuri NR, Holden PJ & James M (2013) Synthesis of deuterated [D 32] oleic acid and its phospholipid derivative [D 64]dioleoyl- sn -glycero-3-phosphocholine. *J Label Compd Radiopharm* **56**, 520–529.
36 Koch HJ & Stuart RS (1977) A novel method for specific labelling of carbohydrates with deuterium by catalytic exchange. *Carbohydr Res* **59**, C1–C6.
37 Hans J & Koch RSS (1978) The synthesis of per-C-deuterated D-glucose. *Carbohydr Res* **64**, 127–134.
38 Koch H & Stuart R (1978) The catalytic C-deuteration of some carbohydrate derivatives. *Carbohydr Res* **67**, 341–348.
39 Hansen S (2012) BayesApp : a web site for indirect transformation of small-angle scattering data. *J Appl Crystallogr* **45**, 566–567.
40 Malik L, Nygaard J, Høiberg-Nielsen R, Arleth L, Hoeg-Jensen T & Jensen KJ (2012) Perfluoroalkyl chains direct novel self-assembly of insulin. *Langmuir* **28**, 593–603.
41 Pedersen JS (1993) Resolution effects and analysis of small-angle neutron scattering data. *Le J Phys IV* **3**, C8-491–C8-498.
42 Mylonas E & Svergun DI (2007) Accuracy of molecular mass determination of proteins in solution by small-angle X-ray scattering. *J Appl Crystallogr* **40**, s245–s249.
43 Michel H, Oesterhelt D & Henderson R (1980) Orthorhombic two-dimensional crystal form of purple membrane. *Proc Natl Acad Sci USA* **77**, 338–342.
44 Rasmussen SGF, Choi H-J, Rosenbaum DM, Kobilka TS, Thian FS, Edwards PC, Burghammer M, Ratnala VRP, Sanishvili R, Fischetti RF *et al.* (2007) Crystal structure of the human beta2 adrenergic G-protein-coupled receptor. *Nature* **450**, 383–387.
45 Schirmer T, Keller TA, Wang YF & Rosenbusch JP (1995) Structural basis for sugar translocation through maltoporin channels at 3.1 A resolution. *Science* **267**, 512–514.
46 Fromme P, Jordan P & Krauß N (2001) Structure of photosystem I. *Biochim Biophys Acta - Bioenerg* **1507**, 5–31.
47 Ben-Shem A, Frolow F & Nelson N (2003) Crystal structure of plant photosystem I. *Nature* **426**, 630–635.
48 Sobolevsky AI, Rosconi MP & Gouaux E (2009) X-ray structure, symmetry and mechanism of an AMPA-subtype glutamate receptor. *Nature* **462**, 745–756.
49 Olesen C, Picard M, Winther A-ML, Gyrup C, Morth JP, Oxvig C, Møller JV & Nissen P (2007) The structural basis of calcium transport by the calcium pump. *Nature* **450**, 1036–1042.
50 Bublitz M, Musgaard M, Poulsen H, Thøgersen L, Olesen C, Schiøtt B, Morth JP, Møller JV & Nissen P (2013) Ion pathways in the sarcoplasmic reticulum Ca2 + -ATPase. *J Biol Chem* **288**, 10759–10765.
51 Putnam CD, Hammel M, Hura GL & Tainer JA (2007) X-ray solution scattering (SAXS) combined with crystallography and computation: defining accurate macromolecular structures, conformations and assemblies in solution. *Q Rev Biophys* **40**, 191–285.
52 Pernot P, Theveneau P, Giraud T, Fernandes RN, Nurizzo D, Spruce D, Surr J, McSweeney S, Round A, Felisaz F *et al.* (2010) New beamline dedicated to solution scattering from biological macromolecules at the ESRF. *J Phys Conf Ser* **247**, 12009.
53 Columbus L (2015) Post-expression strategies for structural investigations of membrane proteins. *Curr Opin Struct Biol* **32**, 131–138.
54 Khoshouei M, Radjainia M, Baumeister W, Danev R (2017) Cryo-EM structure of haemoglobin at 3.2 Å determined with the Volta phase plate. *Nat Commun* **8**, 16099. https://doi.org/10.1038/ncomms16099
55 Maslennikov I & Choe S (2013) Advances in NMR structures of integral membrane proteins. *Curr Opin Struct Biol* **23**, 555–562.
56 Calcutta A, Jessen CM, Behrens MA, Oliveira CLP, Renart ML, González-Ros JM, Otzen DE, Pedersen JS, Malmendal A & Nielsen NC (2012) Mapping of unfolding states of integral helical membrane proteins by GPS-NMR and scattering techniques: TFE-induced unfolding of KcsA in DDM surfactant. *Biochim Biophys Acta* **1818**, 2290–2301.
57 Døvling Kaspersen J, Moestrup Jessen C, Stougaard Vad B, Skipper Sørensen E, Kleiner Andersen K, Glasius M, Pinto Oliveira CL, Otzen DE & Pedersen JS (2014) Low-resolution structures of OmpA·DDM protein-detergent complexes. *ChemBioChem* **15**, 2113–2124.
58 Berthaud A, Manzi J, Pérez J & Mangenot S (2012) Modeling detergent organization around aquaporin-0 using small-angle X-ray scattering. *J Am Chem Soc* **134**, 10080–10088.
59 Bu Z & Engelman DM (1999) A method for determining transmembrane helix association and orientation in detergent micelles using small angle x-ray scattering. *Biophys J* **77**, 1064–1073.
60 Skar-Gislinge N, Simonsen JB, Mortensen K, Feidenhans'l R, Sligar SG, Lindberg Møller B, Bjørnholm T & Arleth L (2010) Elliptical structure of phospholipid bilayer nanodiscs encapsulated by scaffold proteins: casting the roles of the lipids and the protein. *J Am Chem Soc* **132**, 13713–13722.
61 Jordan A, Jacques M, Merrick C, Devos J, Forsyth VT, Porcar L & Martel A (2016) SEC-SANS: size exclusion chromatography combined *in situ* with small-angle neutron scattering. *J Appl Crystallogr* **49**, 2015–2020.
62 Glasoe PK & Long FA (1960) Use of glass electrodes to measure acidities in deuterium oxide. *J Phys Chem* **64**, 188–190.

63 Armarego WLF & Perrin DD (1996) *Purification of Laboratory Chemicals*, 4th edn. Elsevier.
64 Gilbert EP, Schulz JC & Noakes TJ (2006) "Quokka"-the small-angle neutron scattering instrument at OPAL. *Phys B Condens Matter* **385–386**, 1180–1182.
65 Franke D & Svergun DI (2009) DAMMIF, a program for rapid ab-initio shape determination in small-angle scattering. *J Appl Crystallogr* **42**, 342–346.
66 Adams PD, Afonine PV, Bunkóczi G, Chen VB, Davis IW, Echols N, Headd JJ, Hung LW, Kapral GJ, Grosse-Kunstleve RW *et al.* (2010) PHENIX: a comprehensive Python-based system for macromolecular structure solution. *Acta Crystallogr Sect D Biol Crystallogr* **66**, 213–221.
67 Lomize MA, Lomize AL, Pogozheva ID & Mosberg HI (2006) OPM: orientations of proteins in membranes database. *Bioinformatics* **22**, 623–625.

Supporting information

Additional Supporting Information may be found online in the supporting information tab for this article.